Published in final edited form as:

Mol Cell Biol. 2025; 45(4): 143-153. doi:10.1080/10985549.2025.2463892.

Transcriptomic analysis uncovers an unfolded protein response in ADNP syndrome

Anna Bieluszewska^{1,2}, Phillip Wulfridge^{1,2}, Kuo-Chen Fang^{1,2}, Yan Hong^{2,4}, Tomoyo Sawada³, Jennifer Erwin³, Hongjun Song^{2,4}, Guo-li Ming⁴, Kavitha Sarma^{1,2,*}

¹Genome Regulation and Cell Signaling Program, The Wistar Institute, Philadelphia PA 19104

²Epigenetics Institute, University of Pennsylvania, Philadelphia PA 19104

³Lieber Institute for Brain Development, Baltimore MD 21205

⁴Department of Neuroscience and Mahoney Institute for Neurosciences, Perelman School of Medicine, University of Pennsylvania, Philadelphia PA 19104

Abstract

Chromatin regulators are frequently mutated in autism spectrum disorders, but in most cases how they cause disease is unclear. Mutations in the activity dependent neuroprotective protein (ADNP) causes ADNP syndrome, which is characterized by intellectual deficiency and developmental delays. To identify mechanisms that contribute to ADNP syndrome, we used induced pluripotent stem cells derived from ADNP syndrome patients as a model to test the effects of syndromic ADNP mutations on gene expression and neurodifferentiation. We found that some ADNP mutations result in truncated ADNP proteins, which displayed aberrant subcellular localization. Gene expression analyses revealed widespread transcriptional deregulation in all tested mutants. Interestingly, mutants that show presence of ADNP fragments show ER stress as evidenced by activation of the unfolded protein response (UPR). The mutants showing the greatest UPR pathway activation associated with the most severe neurodifferentiation and survival defects. Our results reveal the potential to explore UPR activation as a new biomarker for ADNP syndrome severity and perhaps also in other ASDs where mutations result in presence of truncated proteins.

Keywords

ADNP syndrome; patient-de	rived induced p	pluripotent stem o	cells; neurodifferentiation	on;
transcriptomics; unfolded pro	otein response			

A.B. performed all the experiments, analyzed all the data, and prepared all the figures. Y.H., H.S. and G-l.M. contributed to differentiation protocols. T.S. and J.E. provided control hiPSC lines. P.W. and K-C.F. performed gene set enrichment analyses with data provided by A.B. K.S. wrote the manuscript with input from all authors.

Competing Interests

The authors declare no competing interests.

^{*}Corresponding author: kavitha@sarmalab.com. Author contributions

Introduction

Many neurodevelopmental disorders are caused by mutations in chromatin regulators ^{1, 2}. Activity dependent neuroprotective protein (ADNP) is a homeodomain containing protein best known as a transcriptional repressor in association with heterochromatin protein 1 (HP1) and chromodomain helicase DNA binding protein 4 (CHD4) ³. ADNP is critical for neuronal differentiation and neurodevelopment ³⁻⁵. In humans, ADNP mutations cause ADNP syndrome, also referred to as Helsmoortel-Van der Aa syndrome ^{6, 7}, a neurodevelopmental disorder associated with intellectual disability, delays in speech development, and other motor dysfunctions ⁸. ADNP is also predicted to be one of the more frequent autism spectrum disorder (ASD) associated genes, accounting for an estimated 0.2% of all autism cases globally ⁶.

ADNP contains nine zinc fingers and a homeodomain ⁹. The N terminus of ADNP mediates its interaction with CHD4 ³. ADNP also contains a PxVxL amino acid motif, which is present in several other chromatin regulators and is necessary for interaction with HP1 ^{10, 11}. The homeodomain of ADNP is important for its localization to chromatin ¹². Interestingly, ADNP was also shown to localize to SINE B2 elements and compete with a subset of CTCF sites which are present within these transposable elements ¹³. ADNP loss allows CTCF binding at SINE B2 and leads to altered organization of topologically associated domains which are thought to help finetune gene expression ¹⁴⁻¹⁷. Indeed, human induced pluripotent stem cell (hiPSC) lines derived from an ADNP syndrome patient show alterations in CTCF occupancy at many genomic sites ¹².

Syndromic nonsense or frameshift mutations occur throughout the length of the ADNP gene, with most mutations occurring in its last exon which encodes 95% of the protein. In almost all cases, these mutations result in loss of the homeodomain and retention of some of the zinc fingers alone. Interestingly, some mutations like Y719*, R730* and N832K fs*81 have been shown to occur more frequently in ADNP syndrome patients, indicating the presence of mutational hotspots ^{18, 19}. Overexpression of these ADNP mutant proteins in different cell types revealed distinct patterns of cellular localization ²⁰⁻²². While some mutants clearly remained nuclear, others became localized to the cytoplasm. In addition to these overexpression studies, some groups have examined the behavior of ADNP proteins in patient-derived samples. Interestingly, in many cases the mutant form of the protein was not detectable ^{12, 23}. This could be due to instability of the truncated ADNP proteins or lack of sensitive reagents to visualize these protein fragments.

ADNP syndrome patients can present with varying degrees of developmental disability ranging from mild to severe ⁶. Previous studies have reported widespread changes in DNA methylation profiles in the peripheral blood of ADNP syndrome patients ²⁴. However, deeper analysis comparing DNA methylation to phenotypic data from ADNP syndrome patients revealed no clear correlation between the extent of changes in DNA methylation and the severity of disease ²⁵. Thus, while episignatures from peripheral blood may have value in diagnosis, they may not be predictive of specific neurodevelopmental outcomes that can aid in early interventional therapies. In this study, we propose that analysis of gene expression profiles from different ADNP mutant cell lines can reveal new biomarkers for the

diagnosis and treatment of ADNP syndrome. We performed a comparative transcriptomic analysis from 4 different ADNP syndrome patient-derived human induced pluripotent stem cell (hiPSC) lines (Table 1) and identify gene expression programs that in some mutants may have more severe consequences to the process of neurodifferentiation than others.

Results

A subset of patient-derived ADNP mutant hiPSCs contain truncated ADNP protein

ADNP syndrome-related mutations are heterozygous frameshifts or nonsense mutations that can result in the expression of truncated proteins. Mutations can occur across the whole coding sequence of the *ADNP* gene with some, including Y719*and N832K fs*81, reported as mutational hotspots ⁸. We acquired 4 different hiPSC lines derived from ADNP syndrome patients (Figure 1A) with the following mutations relative to the cDNA sequence: c.819delC, c.2156insA, c.2287delT, and c.2496_2499delTAAA. These mutations encode for the following ADNP protein products, respectively: K274N fs*31, Y719*, S763P fs*9, and N832K fs*81 (Table 1). All mutations in our ADNP mutant hiPSC lines are located in the last exon, which encodes the majority of the ADNP protein, and the resulting transcripts are expected to escape nonsense-mediated decay ⁶. To confirm this, we analyzed ADNP mRNA levels from RNA-seq and found that ADNP is expressed similarly between control ²⁶ and all ADNP mutant hiPSC lines (Figure 1B).

To evaluate ADNP protein levels in mutant hiPSCs, we performed a western blot in whole cell extracts from these cell lines. For these experiments, we also included a control and Y719* mutant hiPSC line derived from a female ADNP syndrome patient. K274N fs*31, Y719*, S763P fs*9, and N832K fs*81 ADNP proteins have a theoretical molecular weight of 35KDa, 80KDa, 86KDa, and 103KDa, respectively. Using an antibody raised against the first 138 amino acids of human ADNP protein (N-term antibody), which is expected to recognize all 4 mutant protein fragments, we found that in addition to the full length ADNP protein, three of the four mutants, K274N fs*31, Y719*, and S763P fs*9, showed specific signal at their expected molecular weights (Figure 1C, red asterisks). In contrast, N832K fs*81 mutants did not show accumulation of a smaller ADNP fragment. We found that K274N fs*31, Y719*, and S763P fs*9 expressed full length ADNP protein (Figure 1C, arrowhead) at slightly lower levels relative to the control sample. In contrast, N832K fs*81 showed similar full length protein levels as control hiPSCs. Thus, our results indicate that some ADNP syndrome causing mutations result in truncated protein fragments that can potentially contribute to ADNP syndrome through a dominant negative mechanism.

Syndromic mutations lead to unique patterns of ADNP subcellular localization.

Next, we sought to evaluate the cellular behavior of the ADNP mutant proteins. Unfortunately, the commercial ADNP N-terminal antibodies which can recognize truncated ADNP proteins by western blot were not suitable for immunofluorescence experiments. As an alternative, we constructed vectors encoding full length ADNP protein and the four mutants fused to EGFP at the C terminus and transfected them into HEK293T. Full length ADNP protein localized exclusively to the nucleus in distinct foci distributed throughout (Figure 2A). This is consistent with the localization pattern observed when full length

ADNP with an HA tag was expressed in HEK293T ²¹. In contrast, K274N fs*31, which is truncated after the first 4 zinc fingers, displayed both nuclear and cytoplasmic localization with small nuclear foci similar to those observed in full length ADNP-transfected cells. Additionally, many K274N fs*31 cells showed a clear, punctate focus next to the nucleus. ADNP Y719*, which lacks a complete nuclear localization signal, was distributed both in the nucleus and in the cytoplasm. Similar to K274N fs*31, cells expressing Y719* showed a strong punctate signal adjacent to the nucleus, but nuclear foci were not observed. We also found that in some cells with very high levels of Y719* expression, the mutant protein was more broadly distributed throughout the cytoplasm (Figure 2B). Both S763P fs*9, which is truncated in the middle of the homeodomain, and N832K fs*81, which contains all nine zinc fingers and the homeodomain, were localized in the nucleus, but showed a more diffuse signal compared to full length ADNP.

We tested whether expression of Y719* mutant that accumulates in the cytoplasm alters the distribution of endogenous full length ADNP. As expected, ADNP-GFP localized to the nucleus and is detected by a C terminus ADNP antibody. We found that in all cells expressing Y719* (Figure 2B, green, lower panels), endogenous ADNP as detected by the C-terminal antibody remained nuclear (Figure 2B, red, lower panels). Our results show that ADNP protein fragments in patient-derived hiPSCs have unique patterns of sub-cellular localization.

Patient-derived ADNP mutant hiPSCs deregulate unique and shared sets of genes

We compared the RNA-seq data from ADNP mutant hiPSCs to a control hiPSC line to identify genes that are differentially expressed in ADNP mutants. Principal component analysis (PCA) indicated that all ADNP mutants displayed distinct gene expression profiles forming clusters separate from the control (Figure 3A). Interestingly, the N832K fs*81 mutant formed a distinct cluster from both control and the other ADNP mutants. Next, we identified differentially expressed genes (DEGs) in the ADNP mutant hiPSCs compared to control and found a large number of genes to be significantly changed in every mutant (Figure 3B). The majority of identified DEGs were differentially expressed in only a subset of mutants, with over 40% of either upregulated or downregulated genes unique to one mutant and less than 10% commonly identified in all four mutants (Figure 3C). We examined overlaps between DEGs identified in each mutant to determine if any lines were more similar in their expression changes compared to others (Figure 3D). Of the four mutants, Y719* and S763P fs*9 had a greater degree of overlap (about 60%) in both upregulated and downregulated DEGs compared to K274N fs*31 and N832K fs*81, suggesting these two ADNP mutations may have a more similar effect on gene expression. N832K fs*81 shared fewer DEGs with the other three mutants, consistent with its separation from the others based on overall transcriptome profiles (Figure 3A). We next examined the annotated functions of the 494 and 422 genes that were upregulated or downregulated, respectively, in all ADNP mutant lines (Supplementary Figures 1A and 1B). Over 25% of DEGs upregulated in all four mutants are associated with cell communication and signaling, while 26% of DEGs downregulated in all mutants are annotated in regulation of transcription and nucleotide metabolic processes (Figure 3E). These may be pathways that

become consistently dysregulated upon ADNP mutation regardless of the specific mutation type, in addition to the other unique pathways that are deregulated by different mutations.

A subset of ADNP mutant hiPSCs show activation of the unfolded protein response

Our results show that all ADNP mutant hiPSCs up- or downregulate unique as well as shared gene sets. To discover pathways that are deregulated in each mutant, we performed Gene Set Enrichment Analysis (GSEA) ^{27, 28}. Each mutant was analyzed separately against the control. Our analysis revealed several gene sets that were significantly upregulated in ADNP mutant hiPSCs and a few that were downregulated in comparison to control hiPSCs (Supplementary Figures 1C to 1F). Comparison of these data showed that K274N fs*31, Y719*, and S763P fs*9 shared many pathways that were upregulated relative to control. In contrast, GSEA of N832K fs*81 identified pathways that were predominantly downregulated and distinct from the other mutants. Upregulated gene sets in K274N fs*31, Y719*, and S763P fs*9 include many pathways important for growth and survival of stem cells including the PI3K/AKT/mTOR signaling pathway, as well as MYC and E2F transcription factor targets. Interestingly, we noticed that the unfolded protein response (UPR) was also activated in K274N fs*31, Y719*, and S763P fs*9, but not in N832K fs*81 (Figure 4A and Supplementary Figures 1C to 1F). The accumulation of misfolded proteins evokes a protective response from cells designed to sequester misfolded proteins and reduce proteotoxic stress. These sequestered proteins accumulate in a pericentriolar membrane-free cytoplasmic inclusion called an aggresome ²⁹. The sub-cellular localization of K274N fs*31 and Y719* proteins as a bright focus adjacent to the nucleus is consistent with the formation of an aggresome structure.

The unfolded protein response is activated through 3 sensors: PERK, IRE1α, and ATF6 ³⁰. PERK activation results in induction of the ATF4 transcription factor which helps upregulate ER stress response genes, but also has a pro-apoptotic role in response to prolonged stress. In addition, PERK mediated phosphorylation of the eIF2a subunit represses protein translation. Activation of IRE1a induces splicing of X-box binding protein 1 (XBP1) mRNA by IRE1 to produce XBP1s, which translocates to the nucleus and activates genes that promote ER biogenesis, encode for chaperones, and decrease ER stress. Finally, cellular stress results in proteolytic cleavage of ATF6 which allows it to translocate from the ER to the nucleus and promote the expression of ER chaperones, ER biogenesis, and genes associated with an inflammatory response. We found that ATF4 mRNA levels trend upward in K274N fs*31, Y719*, and S763P fs*9, but are closer to control levels in N832K fs*81 (Figure 4B). Similarly, XBP1 mRNA levels are elevated in K274N fs*31, Y719*, and S763P fs*9, but not in N832K fs*81 (Figure 4B). ATF6 mRNA levels remain unchanged in K274N fs*31, Y719*, and S763P fs*9 compared to control hiPSCs. We examined the protein levels of some of the main players in the UPR pathway, such as PERK and XBP1, and did not observe an increase in protein levels in the ADNP mutant lines (Supplementary Figure 1G). It is possible that at the hiPSC stage we only observe a transcriptomic response and that increases in UPR pathway proteins only occur with further pathway activation upon differentiation. To test whether ADNP mutations which result in a truncated fragment elicit a broader ER stress response, we analyzed a larger set of 112 genes linked to the UPR pathway that we obtained from MsigDB ³¹. We found that compared to controls, K274N

fs*31, Y719*, and S763P fs*9 showed upregulation of most of these genes, but N832K fs*81 did not (Figure 4C). Together our results reveal an activated unfolded protein response signature specifically in ADNP mutant hiPSCs that show presence of truncated fragments.

Effects of ADNP mutations on neurodifferentiation

Next, we tested the neurodifferentiation potential of ADNP mutant hiPSCs. We chose to exclude the control and Y719* female hiPSC lines from the neurodifferentiation experiments because these were reprogrammed differently from the 5 male lines, proliferated slowly, and showed an increased number of cells that appeared differentiated in culture. We first confirmed that undifferentiated control and ADNP mutant hiPSCs look similar (Supplementary Figure 2A). Proliferation of control and ADNP mutant hiPSC lines was similar and all cell lines grew as colonies characteristic of hiPSCs, with smooth well-defined margins and no clear borders between the cells within colonies. All hiPSC lines also expressed high levels of pluripotency markers such as *POU5F1* and *SOX2* (Supplementary Figure 2B).

We induced hiPSC differentiation to neuronal progenitor cells (NPCs) using a three-stage protocol (Supplementary Figure 2C). To obtain NPCs, dissociated single cells derived from control and K274N fs*31, Y719*, S763P fs*9, and N832K fs*81 hiPSCs were aggregated with AggreWell-800 plates to generate embryoid bodies (EBs) of similar size and morphology. In the first stage of differentiation, EBs showed a lack of shape heterogeneity. The only noticeable difference was in the size of Y719* and N832K fs*81 EBs, which appeared slightly larger than control (Figure 5A, upper panel). At day 16, control, K274N fs*31, Y719*, and N832K fs*81 EBs remained viable and were visibly larger compared to their size in the first stage of differentiation (Figure 5A, lower panel). In contrast, S763P fs*9 mutant EBs spontaneously dissociated starting around day 5, and despite repeated attempts these mutants consistently did not survive past day 15, with no viable cells present by the last stage of differentiation (D16-D23). At the final stage, EBs were dissociated and NPCs were grown as a monolayer (Figure 5B). We observed that while K274N fs*31 had similar appearance to controls at this stage, Y719* grew markedly slower, while N832K fs*81 showed a more heterogeneous population of cells compared to control with smaller cells resembling control NPCs surrounded by other, larger cells (Figure 5B, lower panel).

We performed RNA-seq analysis of NPCs to analyze the expression of well-known neural lineage markers such as Paired box 6 (PAX6), Neuregulin 1 (NRG1), and Nestin (NES). PAX6 is a highly conserved transcription factor whose functions are essential for neuronal stem cell proliferation and central nervous system development. NRG1 is a membrane glycoprotein that is important for cell-cell signaling and synaptic transmission. NES is an intermediate filament expressed in undifferentiated central nervous system cells, including neural progenitors. While all cell lines had comparable levels of NES expression, NRG1 and PAX6 showed decreased expression in ADNP mutant lines compared to control (Figure 5C). Immunofluorescence with PAX6 antibody in NPCs revealed reduced signal intensity in all ADNP mutants compared to control NPCs (Figure 5D). Interestingly, N832K fs*81 NPCs

showed PAX6 positive signal only in cells that resembled control NPCs, and not in the larger cells of unknown lineage.

We performed a deeper analysis of our RNA-seq data from ADNP mutants at the NPC stage (Figure 6, Supplementary Table 3). Surprisingly, K274N fs*31 and Y719* show relatively few differentially expressed genes (DEGs) (175 and 398, respectively) (Figure 6A, left and middle). One potential explanation for this is that our RNA-seq only captures cells that successfully survive differentiation, while cells that die during the process, for example due to UPR-induced apoptosis, would drop out of the sample. Consistent with this, we did not observe enrichment of UPR pathway genes in the small set of DEGs in K274N fs*31 and Y719*. In contrast, we identified 4,665 DEGs in the N832K fs*81 mutant (Figure 6A, right). Gene ontology analysis of these DEGs revealed that pathways associated with neural signatures are generally downregulated, while pathways for mesodermal differentiation processes such as "vasculature and circulatory system development" are upregulated (Figure 6B). This suggests that the N832K fs*81 ADNP mutation results in non-specific differentiation towards other lineages, which is supported by the heterogeneous nature of N832K fs*81 at the NPC stage. Thus, ADNP mutations result in compromised neurodifferentiation, with mutants showing the greatest UPR pathway activation (Y719* and S763P fs*9) associated with the most severe cell differentiation and survival defects.

Discussion

In this study, we used ADNP syndrome patient-derived human induced pluripotent cells (hiPSC) to test how different ADNP mutations impact protein distribution, gene expression, and neurodifferentiation. The ADNP mutations examined in this study have distinct consequences on cellular localization, with K274N fs*31, Y719*, and S763P fs*9 truncated proteins being present in the cell, and N832K fs*81 being unstable and consequently degraded. To our knowledge, this is the first report of presence of ADNP truncated proteins in cells from a subset of ADNP syndrome patients.

Mutations in ADNP can affect gene expression in different ways. Loss of ADNP localization to chromatin can impact the localization of several important epigenetic regulators that are recruited to chromatin through their interactions with ADNP. These include CHD4, BRG1 $^{12,\,32}$, and HP1. However, the presence of ADNP fragments has additional implications for its molecular interactions. K274N fs*31, Y719*, and S763P fs*9 mutants retain the first 250 amino acids of ADNP, which were shown to contain the domain mediating interaction with CHD4 3 . These mutants can potentially affect the expression of genes regulated by CHD4 by sequestering CHD4 away from chromatin.

Previous studies analyzing a cohort of ADNP syndrome patients identified Y719* as a frequently occurring mutation and also reported that patients with this mutation were more severely affected than others ⁸. In an independent study, expression of mouse ADNP Y718* mutant (the equivalent of human Y719*) in neuroblastoma cell lines and their subsequent differentiation into neuron-like cells showed an increased cell death phenotype ²². Overexpression of both K274N fs*31 and Y719* ADNP proteins in HEK293 results in their accumulation adjacent to the nucleus (Figure 2), indicating the formation of a

protective aggresome structure. Interestingly, through transcriptomic analysis in ADNP mutant hiPSCs, we discovered an upregulation of the unfolded protein response (UPR) in K274N fs*31, Y719*, and S763P fs*9 mutants. Neurodifferentiation of ADNP mutant hiPSCs into neural progenitors was most strongly impaired in S763P fs*9 mutant cells followed by Y719*. Notably, S763P fs*9 showed the highest upregulation of the UPR, and S763P fs*9 protein failed to form an aggresome structure when expressed in HEK293T. It is possible that the inability to sequester misfolded proteins in an aggresome makes S763P fs*9 mutant hiPSCs more susceptible to cellular stress, thereby diminishing survival upon neurodifferentiation.

Phosphorylation of the translation initiation factor eIF2a through chronic activation of PERK can also result in a general suppression of protein synthesis. The critical importance of the ER in cells with secretory function, including neurons, coupled with the reduced production of secreted proteins that are important for nervous system homeostasis may also contribute to the significant death observed in S763P fs*9 during neurodifferentiation.

Peripheral blood is frequently used as a source for biomarker discovery for many diseases because of ease of access. DNA methylation analysis from the peripheral blood of ADNP syndrome patients identified unique episignatures based on mutation ²⁴, but did not correlate with severity of disease ²⁵. Our discovery of UPR activation in a subset of ADNP syndrome patient hiPSCs, together with the observed tendency of these mutant proteins to accumulate in aggresomes in HEK293 cells, represents a molecular signature that may also be detectable in non-neuronal cells including peripheral blood. Analysis of the peripheral blood transcriptome from an expanded cohort of ADNP syndrome patients may help establish the UPR as a new biomarker for disease severity that can aid in the stratification of patients for early interventional therapy.

Chronic ER stress and activation of the UPR have been reported in several neurodegenerative diseases, including Alzheimer's disease and Parkinson's disease (reviewed in ³³), where they are reported to be early markers of disease. Because of the high incidence of neurodegenerative diseases, development of gene therapy and pharmacological intervention strategies to alleviate ER stress is already well underway. Identifying the presence of pathogenic truncated protein fragments that cause ER stress in ADNP syndrome and other autism spectrum disorders can provide a rationale for repurposing therapeutic strategies developed for neurodegenerative diseases toward interventional therapies for some neurodevelopmental disorders.

Materials and methods

Cell lines and cell culture

ADNP mutant hiPSC lines were acquired from the Simons Foundation Autism Research Initiative (SFARI). All cell lines were cultured at 37 °C in a humidified atmosphere containing 5% CO₂. Human iPSCs were cultured on Geltrex (ThermoFisher, A14133020) coated plates in StemMACS iPS Brew-XF medium (Miltenyi Biotec, 130-104-368). Cells were subcultured every 4-5 days with Versene solution (ThermoFisher, 15040066). HEK293T cells were grown in DMEM supplemented with 10% calf serum (Gibco), 1X

MEM non-essential amino acids (Gibco 11140), 1X GlutaMAX (Gibco 35050), 25 mM HEPES, 100 U/ml Pen-Strep, and 55 μ M 2-mercaptoethanol (Gibco, 21985023).

Plasmid construction

pRP-TET-ON expression vectors encoding full-length (WT) ADNP and truncated ADNP mutants (K274N fs*31, Y719*, S763P fs*9, and N832K fs*81) were ordered via Vector Builder. To generate constructs expressing WT and mutant ADNP with C-terminal EGFP, the coding sequences were amplified from pRP-TET-ON vectors, and the EGFP sequence was amplified from the pEGFP-C2 vector with Q5 polymerase (NEB, M0491L). NEBuilder (NEB, E2621L) was then used to assemble constructs into the pLV backbone (Vector Builder).

Antibodies

The following primary antibodies were used: anti-PAX6 (Proteintech, 12323-1-AP), anti-ADNP (F-9, sc-376674), anti-ADNP (Sarma lab, ¹²), anti-Actin (Millipore Sigma A2066).

Differentiating human iPSCs into NPCs

Human iPSCs were dissociated with Accutase (gibco) and $3x10^6$ cells were aggregated to form embryoid body (EBs) by Aggrewell (STEMCELL Technologies). The following day (Day 1), EBs were gently collected from the Aggrewell plate and transferred into 6-well plate and grown in H1 medium rotating at 110 rpm until day 6. During days 1-6 half of the media was changed daily. From day 7-15, EBs were grown in H2 medium rotating at 110 rpm with half of the medium changed daily. On day 16, EBs were dissociated with Accutase into single cells and $2x10^6$ cells were plated on Matrigel (Corning) coated 6-well plate for neural progenitor cells expansion in H3 medium until day 23 with half of the medium changed daily (unpublished method).

Immunofluorescence

For immunostaining PAX6 in NPCs, cells were grown on a coverslip coated with Geltrex. Cells were fixed with 4% paraformaldehyde for 15 minutes at room temperature. The samples were washed with DPBS at room temperature and incubated with blocking buffer (0.1% Triton-100, 1% BSA in DPBS) for 30 minutes. Both antibodies, primary and secondary, were diluted in the blocking solution. 293T cells transfected with plasmids encoding either wild type or ADNP mutant, were fixed with 4% paraformaldehyde for 15 minutes at room temperature, and processed as described previously ³⁴.

Sample preparation for western blot, RNA-seq and library generation

Whole-cell extracts were prepared by lysing cells in RIPA buffer (50 mM Tris HCl pH 8, 150 mM NaCl, 1% NP-40, 0.5% sodium deoxycholate, 0.1% SDS) supplemented with protease inhibitors. After 20 minutes on ice, samples were briefly sonicated and centrifuged at $10,000 \times g$ for 15 min at 4°C to remove cell debris.

RNA was extracted from undifferentiated hiPSCs and NPCs using Trizol LS Reagent (Invitrogen, 10296010), subjected to DNase digestion with Turbo DNase (Ambion AM2238), and rRNA-depleted using FastSelect -rRNA HMR (Qiagen, 334387). Ultra II

Directional RNA Library Prep Kit (NEB, E7760) was used to convert RNA to cDNA. cDNA samples were end-repaired with End-Repair Mix (Enzymatics, Y9140-LC-L), A-tailed using Klenow exonuclease minus (Enzymatics, P7010-HC-L), purified with MinElute columns (Qiagen), and ligated to Illumina adapters (NEB, E7600) with T4 DNA ligase (Enzymatics, L6030-HC-L). Size selection for fragments >150 bp was performed using AMPure XP beads (Beckman Coulter, A63881). Libraries were PCR amplified with barcoded adapters for Illumina sequencing (NEB, E7600) using Q5 DNA polymerase (NEB, M0491) and purified with MinElute. Sequencing was performed on a NextSeq500 instrument (Illumina) with 38x2 paired-end cycles for hiPSC samples and on a NextSeq2000 instrument (Illumina) with 61x2 paired-end cycles for NPC samples.

Sequencing alignment and processing

RNA-Seq data were aligned to hg38 using STAR version 2.7.9a-GCC-11.2.0 ³⁵. RSEM version 1.3.3-foss-2022a ³⁶was used to obtain estimated counts. Differential analysis was performed in R version 4.1.3 using packages limma version 3.50.3³⁷ and edgeR version 3.36.0 ³⁸. For RNA-Seq differential analysis, genes with low expression were removed with the built-in edgeR function "filterByExpr". Differentially expressed genes were defined by using a cutoff of adjusted p-val <= 0.05. The pheatmap R package (version 1.0.12) was used to generate RNA-seq heatmaps. Venn diagrams of gene list overlaps were generated using official gene symbol names with the InteractiVenn tool ³⁹. Gene ontology analysis was performed using DAVID with official gene symbol names as input ^{40, 41}. Gene enrichment set analysis was performed using GSEA software ^{27, 28} with transcript per million (TPM) values as input.

Supplementary Material

Refer to Web version on PubMed Central for supplementary material.

Acknowledgments

This work was supported by funding from the NIH: R01NS135217, R01GM143229, and R21MH123753 to K.S., R35NS116843 to H.S., and R35NS097370 to G-l.M.; and by a grant from the Simons Foundation Autism Research Initiative (670739) to K.S.

Data Access

All FASTQs and RNA-Seq counts generated during this project have been uploaded to GEO with accession code GSE280293. https://www.ncbi.nlm.nih.gov/geo/query/acc.cgi?acc=GSE280293

All supplementary data tables are available on Mendeley. https://data.mendeley.com/preview/kxyxdsz84v?a=9b6b986d-9174-4ecb-929d-54ce8e8983f9

REFERENCES

1. Lewis EM, Kroll KL. Development and disease in a dish: The epigenetics of neurodevelopmental disorders. Epigenomics. 2018;10:219–231. doi: 10.2217/epi-2017-0113. [PubMed: 29334242]

 Mastrototaro G, Zaghi M, Sessa A. Epigenetic mistakes in neurodevelopmental disorders. J Mol Neurosci. 2017;61:590–602. doi: 10.1007/s12031-017-0900-6. [PubMed: 28255957]

- 3. Ostapcuk V, Mohn F, Carl SH, Basters A, Hess D, Iesmantavicius V, Lampersberger L, Flemr M, Pandey A, Thoma NH, et al. Activity-dependent neuroprotective protein recruits hp1 and chd4 to control lineage-specifying genes. Nature. 2018;557:739–743. doi: 10.1038/s41586-018-0153-8. [PubMed: 29795351]
- 4. Sun X, Peng X, Cao Y, Zhou Y, Sun Y. Adnp promotes neural differentiation by modulating wnt/beta-catenin signaling. Nat Commun. 2020;11:2984. doi: 10.1038/s41467-020-16799-0. [PubMed: 32533114]
- Pinhasov A, Mandel S, Torchinsky A, Giladi E, Pittel Z, Goldsweig AM, Servoss SJ, Brenneman DE, Gozes I. Activity-dependent neuroprotective protein: A novel gene essential for brain formation. Brain Res Dev Brain Res. 2003;144:83–90. doi: 10.1016/s0165-3806(03)00162-7.
 [PubMed: 12888219]
- 6. Helsmoortel C, Vulto-van Silfhout AT, Coe BP, Vandeweyer G, Rooms L, van den Ende J, Schuurs-Hoeijmakers JH, Marcelis CL, Willemsen MH, Vissers LE, et al. A swi/snf-related autism syndrome caused by de novo mutations in adnp. Nat Genet. 2014;46:380–384. doi: 10.1038/ng.2899. [PubMed: 24531329]
- 7. Vandeweyer G, Helsmoortel C, Van Dijck A, Vulto-van Silfhout AT, Coe BP, Bernier R, Gerdts J, Rooms L, van den Ende J, Bakshi M, et al. The transcriptional regulator adnp links the baf (swi/snf) complexes with autism. Am J Med Genet C Semin Med Genet. 2014;166C:315–326. doi: 10.1002/ajmg.c.31413. [PubMed: 25169753]
- Van Dijck A, Vulto-van Silfhout AT, Cappuyns E, van der Werf IM, Mancini GM, Tzschach A, Bernier R, Gozes I, Eichler EE, Romano C, et al. Clinical presentation of a complex neurodevelopmental disorder caused by mutations in adnp. Biol Psychiatry. 2019;85:287–297. doi: 10.1016/j.biopsych.2018.02.1173. [PubMed: 29724491]
- Zamostiano R, Pinhasov A, Gelber E, Steingart RA, Seroussi E, Giladi E, Bassan M, Wollman Y, Eyre HJ, Mulley JC, et al. Cloning and characterization of the human activity-dependent neuroprotective protein. J Biol Chem. 2001;276:708–714. doi: 10.1074/jbc.M007416200. [PubMed: 11013255]
- Ahel J, Pandey A, Schwaiger M, Mohn F, Basters A, Kempf G, Andriollo A, Kaaij L, Hess D, Buhler M. Chahp2 and chahp control diverse retrotransposons by complementary activities. Genes Dev. 2024;38:554–568. doi: 10.1101/gad.351769.124. [PubMed: 38960717]
- 11. Lechner MS, Schultz DC, Negorev D, Maul GG, Rauscher FJ, 3rd. The mammalian heterochromatin protein 1 binds diverse nuclear proteins through a common motif that targets the chromoshadow domain. Biochem Biophys Res Commun. 2005;331:929–937. doi: 10.1016/j.bbrc.2005.04.016. [PubMed: 15882967]
- 12. Yan Q, Wulfridge P, Doherty J, Fernandez-Luna JL, Real PJ, Tang HY, Sarma K. Proximity labeling identifies a repertoire of site-specific r-loop modulators. Nat Commun. 2022;13:53. doi: 10.1038/s41467-021-27722-6. [PubMed: 35013239]
- 13. Kaaij LJT, Mohn F, van der Weide RH, de Wit E, Buhler M. The chahp complex counteracts chromatin looping at ctcf sites that emerged from sine expansions in mouse. Cell. 2019;178:1437–1451 e1414. doi: 10.1016/j.cell.2019.08.007. [PubMed: 31491387]
- Bonev B, Cavalli G. Organization and function of the 3d genome. Nat Rev Genet. 2016;17:661–678. doi: 10.1038/nrg.2016.112. [PubMed: 27739532]
- 15. Dekker J, Mirny L. The 3d genome as moderator of chromosomal communication. Cell. 2016;164:1110–1121. doi: 10.1016/j.cell.2016.02.007. [PubMed: 26967279]
- 16. Dixon JR, Gorkin DU, Ren B. Chromatin domains: The unit of chromosome organization. Mol Cell. 2016;62:668–680. doi: 10.1016/j.molcel.2016.05.018. [PubMed: 27259200]
- 17. Rowley MJ, Corces VG. Organizational principles of 3d genome architecture. Nat Rev Genet. 2018;19:789–800. doi: 10.1038/s41576-018-0060-8. [PubMed: 30367165]
- 18. D'Incal CP, Van Rossem KE, De Man K, Konings A, Van Dijck A, Rizzuti L, Vitriolo A, Testa G, Gozes I, Vanden Berghe W, et al. Chromatin remodeler activity-dependent neuroprotective protein (adnp) contributes to syndromic autism. Clin Epigenetics. 2023;15:45. doi: 10.1186/s13148-023-01450-8: [PubMed: 36945042]

 Van Dijck A, Vulto-van Silfhout AT, Cappuyns E, van der Werf IM, Mancini GM, Tzschach A, Bernier R, Gozes I, Eichler EE, Romano C, et al. Clinical presentation of a complex neurodevelopmental disorder caused by mutations in adnp. Biol Psychiatry. 2019;85:287–297. doi: 10.1016/j.biopsych.2018.02.1173. [PubMed: 29724491]

- 20. Cappuyns E, Huyghebaert J, Vandeweyer G, Kooy RF. Mutations in adnp affect expression and subcellular localization of the protein. Cell Cycle. 2018;17:1068–1075. doi: 10.1080/15384101.2018.1471313. [PubMed: 29911927]
- 21. Ge C, Tian Y, Hu C, Mei L, Li D, Dong P, Zhang Y, Li H, Sun D, Peng W, et al. Clinical impact and in vitro characterization of adnp variants in pediatric patients. Mol Autism. 2024;15:5. doi: 10.1186/s13229-024-00584-7. [PubMed: 38254177]
- Ganaiem M, Karmon G, Ivashko-Pachima Y, Gozes I. Distinct impairments characterizing different adnp mutants reveal aberrant cytoplasmic-nuclear crosstalk. Cells. 2022;11. doi: 10.3390/ cells11192994.
- 23. D'Incal CP, Cappuyns E, Choukri K, De Man K, Szrama K, Konings A, Bastini L, Van Meel K, Buys A, Gabriele M, et al. Tracing the invisible mutant adnp protein in helsmoortel-van der aa syndrome patients. Sci Rep. 2024;14:14710. doi: 10.1038/s41598-024-65608-x. [PubMed: 38926592]
- 24. Bend EG, Aref-Eshghi E, Everman DB, Rogers RC, Cathey SS, Prijoles EJ, Lyons MJ, Davis H, Clarkson K, Gripp KW, et al. Gene domain-specific DNA methylation episignatures highlight distinct molecular entities of adnp syndrome. Clin Epigenetics. 2019;11:64. doi: 10.1186/s13148-019-0658-5. [PubMed: 31029150]
- 25. Breen MS, Garg P, Tang L, Mendonca D, Levy T, Barbosa M, Arnett AB, Kurtz-Nelson E, Agolini E, Battaglia A, et al. Episignatures stratifying helsmoortel-van der aa syndrome show modest correlation with phenotype. Am J Hum Genet. 2020;107:555–563. doi: 10.1016/j.ajhg.2020.07.003. [PubMed: 32758449]
- 26. Sawada T, Benjamin KJM, Brandtjen AC, Tietze E, Allen SJ, Paquola ACM, Kleinman JE, Hyde TM, Erwin JA. Generation of four postmortem dura-derived ips cell lines from four control individuals with genotypic and brain-region-specific transcriptomic data available through the brainseq consortium. Stem Cell Res. 2020;46:101806. doi: 10.1016/j.scr.2020.101806. [PubMed: 32446240]
- 27. Mootha VK, Lindgren CM, Eriksson KF, Subramanian A, Sihag S, Lehar J, Puigserver P, Carlsson E, Ridderstrale M, Laurila E, et al. Pgc-1alpha-responsive genes involved in oxidative phosphorylation are coordinately downregulated in human diabetes. Nat Genet. 2003;34:267–273. doi: 10.1038/ng1180. [PubMed: 12808457]
- 28. Subramanian A, Tamayo P, Mootha VK, Mukherjee S, Ebert BL, Gillette MA, Paulovich A, Pomeroy SL, Golub TR, Lander ES, et al. Gene set enrichment analysis: A knowledge-based approach for interpreting genome-wide expression profiles. Proc Natl Acad Sci U S A. 2005;102:15545–15550. doi: 10.1073/pnas.0506580102. [PubMed: 16199517]
- 29. Johnston JA, Ward CL, Kopito RR. Aggresomes: A cellular response to misfolded proteins. J Cell Biol. 1998;143:1883–1898. doi: 10.1083/jcb.143.7.1883. [PubMed: 9864362]
- 30. Hetz C, Zhang K, Kaufman RJ. Mechanisms, regulation and functions of the unfolded protein response. Nat Rev Mol Cell Biol. 2020;21:421–438. doi: 10.1038/s41580-020-0250-z. [PubMed: 32457508]
- 31. Liberzon A, Birger C, Thorvaldsdottir H, Ghandi M, Mesirov JP, Tamayo P. The molecular signatures database (msigdb) hallmark gene set collection. Cell Syst. 2015;1:417–425. doi: 10.1016/j.cels.2015.12.004. [PubMed: 26771021]
- 32. Sun X, Yu W, Li L, Sun Y. Adnp controls gene expression through local chromatin architecture by association with brg1 and chd4. Front Cell Dev Biol. 2020;8:553. doi: 10.3389/fcell.2020.00553. [PubMed: 32714933]
- 33. Hetz C, Saxena S. Er stress and the unfolded protein response in neurodegeneration. Nat Rev Neurol. 2017;13:477–491. doi: 10.1038/nrneurol.2017.99. [PubMed: 28731040]
- 34. Bieluszewska A, Wulfridge P, Doherty J, Ren W, Sarma K. Atrx histone binding and helicase activities have distinct roles in neuronal differentiation. Nucleic Acids Res. 2022 doi:10.1093/nar/gkac683. doi: 10.1093/nar/gkac683.

35. Dobin A, Davis CA, Schlesinger F, Drenkow J, Zaleski C, Jha S, Batut P, Chaisson M, Gingeras TR. Star: Ultrafast universal rna-seq aligner. Bioinformatics. 2013;29:15–21. doi: 10.1093/bioinformatics/bts635. [PubMed: 23104886]

- 36. Li B, Dewey CN. Rsem: Accurate transcript quantification from rna-seq data with or without a reference genome. BMC Bioinformatics. 2011;12:323. doi: 10.1186/1471-2105-12-323. [PubMed: 21816040]
- 37. Ritchie ME, Phipson B, Wu D, Hu Y, Law CW, Shi W, Smyth GK. Limma powers differential expression analyses for rna-sequencing and microarray studies. Nucleic Acids Res. 2015;43:e47. doi: 10.1093/nar/gkv007. [PubMed: 25605792]
- 38. Robinson MD, McCarthy DJ, Smyth GK. Edger: A bioconductor package for differential expression analysis of digital gene expression data. Bioinformatics. 2010;26:139–140. doi: 10.1093/bioinformatics/btp616. [PubMed: 19910308]
- 39. Heberle H, Meirelles GV, da Silva FR, Telles GP, Minghim R. Interactivenn: A web-based tool for the analysis of sets through venn diagrams. BMC Bioinformatics. 2015;16:169. doi: 10.1186/s12859-015-0611-3. [PubMed: 25994840]
- 40. Huang da W, Sherman BT, Lempicki RA. Systematic and integrative analysis of large gene lists using david bioinformatics resources. Nat Protoc. 2009;4:44–57. doi: 10.1038/nprot.2008.211. [PubMed: 19131956]
- 41. Sherman BT, Hao M, Qiu J, Jiao X, Baseler MW, Lane HC, Imamichi T, Chang W. David: A web server for functional enrichment analysis and functional annotation of gene lists (2021 update). Nucleic Acids Res. 2022 doi:10.1093/nar/gkac194. doi: 10.1093/nar/gkac194.

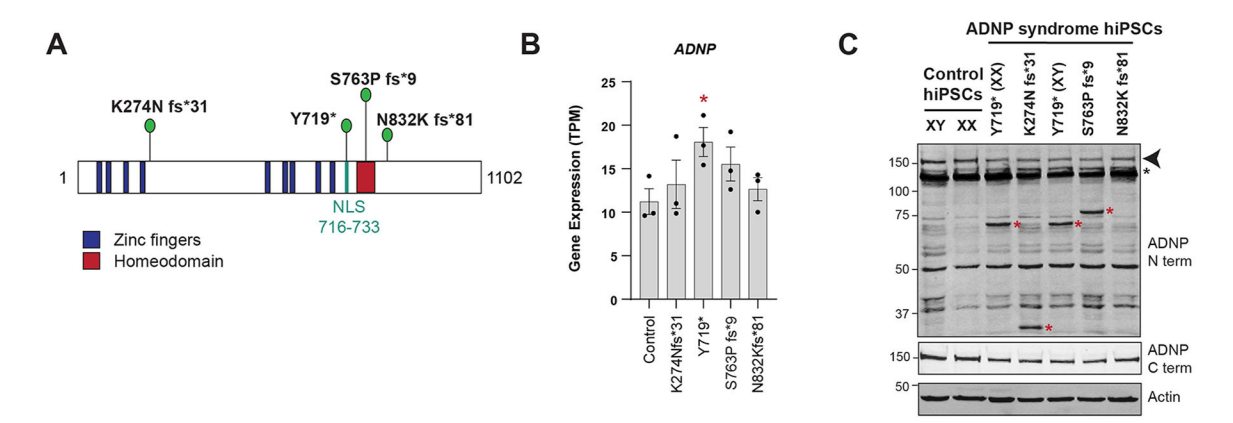
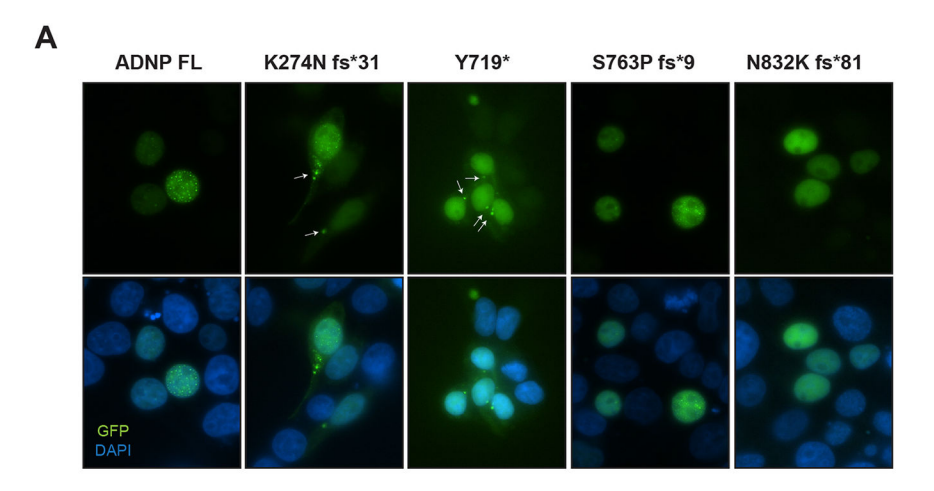


Figure 1. Patient-derived ADNP syndrome hiPSCs show presence of ADNP mutant fragments.

- A. Schematic of full-length ADNP showing protein domains and the locations of mutations in this study.
- B. Bar plot of RNA-seq expression of *ADNP* in transcripts per million (TPM) in different hiPSC lines as indicated. Dots indicate 3 independent biological replicates. Data are presented as mean values $\pm SEM$.
- C. Western blot for ADNP using an N-terminal antibody recognizing the first 138 amino acids of ADNP in different hiPSC lines as indicated above the panel. Actin was used as a loading control. The arrowhead indicates full length ADNP. The red asterisks mark the location of truncated ADNP fragments, and the black asterisk denotes a non-specific band detected by this antibody.



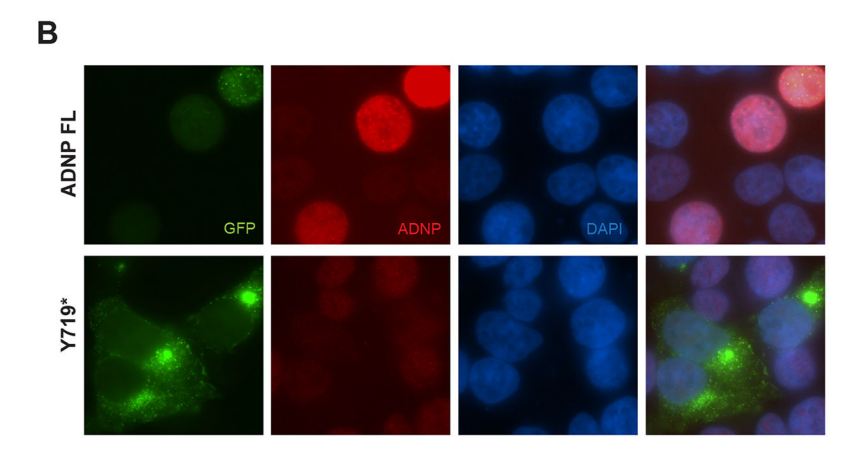


Figure 2. Truncated ADNP proteins show different patterns of subcellular localization. A. Representative images showing subcellular localization of EGFP-fused ADNP full length (FL), K274N fs*31, Y719*, S763P fs*9, and N832K fs*81 (green) in 293T cells. Nuclei are stained with DAPI (blue).

B. Representative images showing subcellular localization of EGFP-fused ADNP full length (FL) and Y719* (green) and endogenous full length ADNP (red) in 293T cells. Nuclei are stained with DAPI (blue).

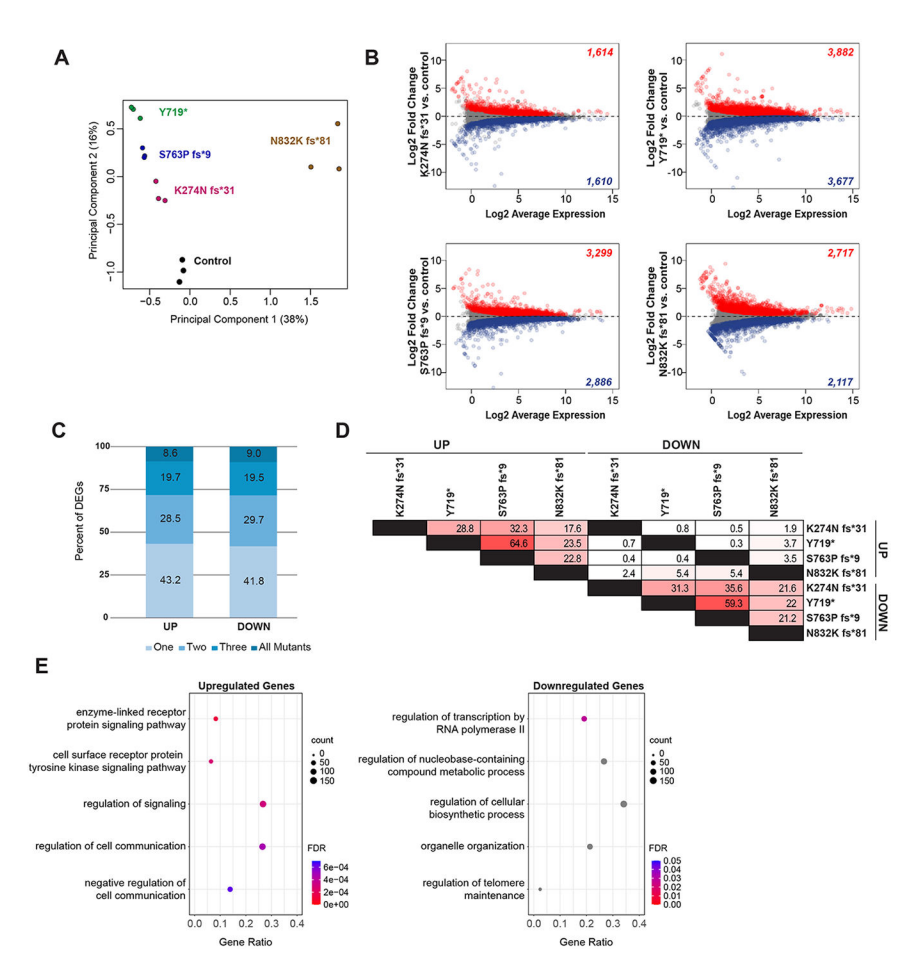


Figure 3. ADNP mutant hiPSCs show widespread changes in gene expression.

- A. Principal component analysis of RNA-seq gene expression (log2 TPM) in control, K274N fs*31, Y719*, S763P fs*9, and N832K fs*81 hiPSCs.
- B. MA plots of RNA-seq differential gene expression analyses between Control and ADNP mutants, as indicated. Red dots and numbers indicate genes significantly upregulated in mutants (adjusted P-value 0.05 and log2 fold change > 0). Blue dots and numbers indicate genes significantly downregulated in mutants (adjusted P-value 0.05 and log2 fold change < 0).
- C. Bar plot showing percentage of differentially expressed genes that are deregulated across one, two, three, or all four ADNP mutant lines.
- D. Heatmap showing percentage of overlap between DEGs (up- and downregulated) in K274N fs*31, Y719*, S763P fs*9, and N832K fs*81 hiPSCs.
- E. Gene ontology of top 5 most significantly up- or downregulated biological processes identified in K274N fs*31, Y719*, S763P fs*9, and N832K fs*81 mutants.

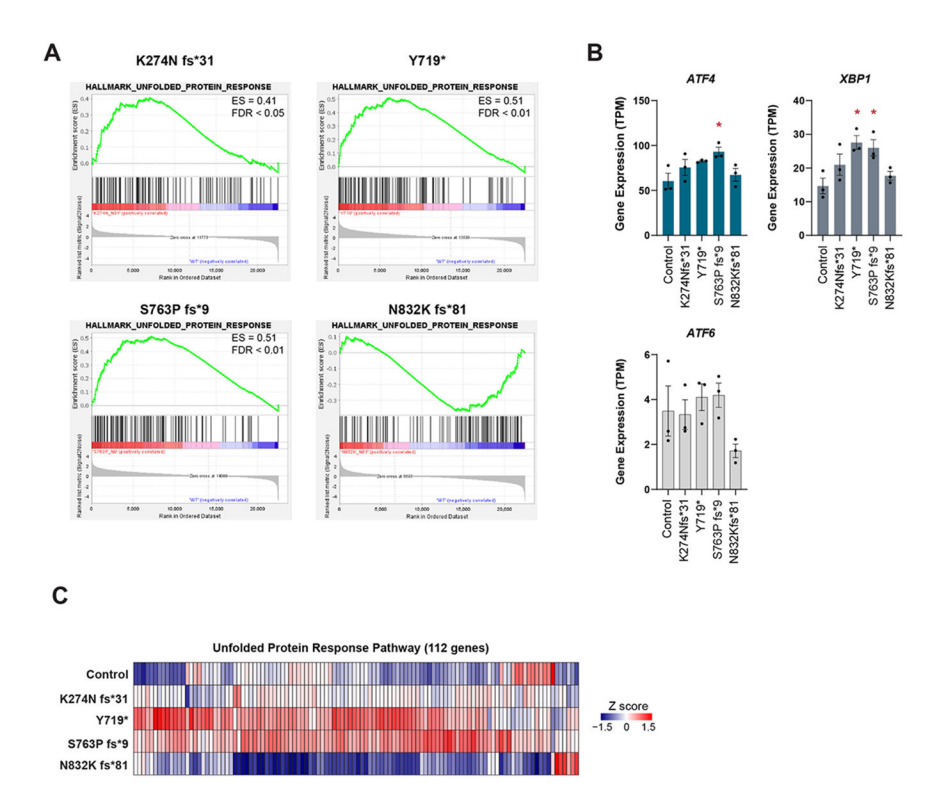


Figure 4. ADNP truncated fragment presence correlates to activation of the unfolded protein response.

- A. Enrichment plot in HALLMARK_UNFOLDED_PROTEIN_RESPONSE for all four mutants. Enrichment score and FDR are indicated for K274N fs*31, Y719*, S763P fs*9 and not significant for N832K fs*81.
- B. Bar plot showing *ATF4*, *XBP1*, and *ATF6* expression in transcripts per million (TPM) in different hiPSC lines as indicated. Dots indicate 3 independent biological replicates. Data are presented as mean values \pm 0.5 EM. * p < 0.05, Welch's t-test.
- C. Heat map of expression of 112 genes related to the unfolded protein response pathway in Control, K274N fs*31, Y719*, S763P fs*9, and N832K fs*81 hiPSCs. Each column represents Z-scores calculated using averaged RNA-seq expression, in transcripts per million (TPM), from three independent biological replicates. Z-scores were computed across Control, K274N fs*31, Y719*, S763P fs*9, and N832K fs*81.

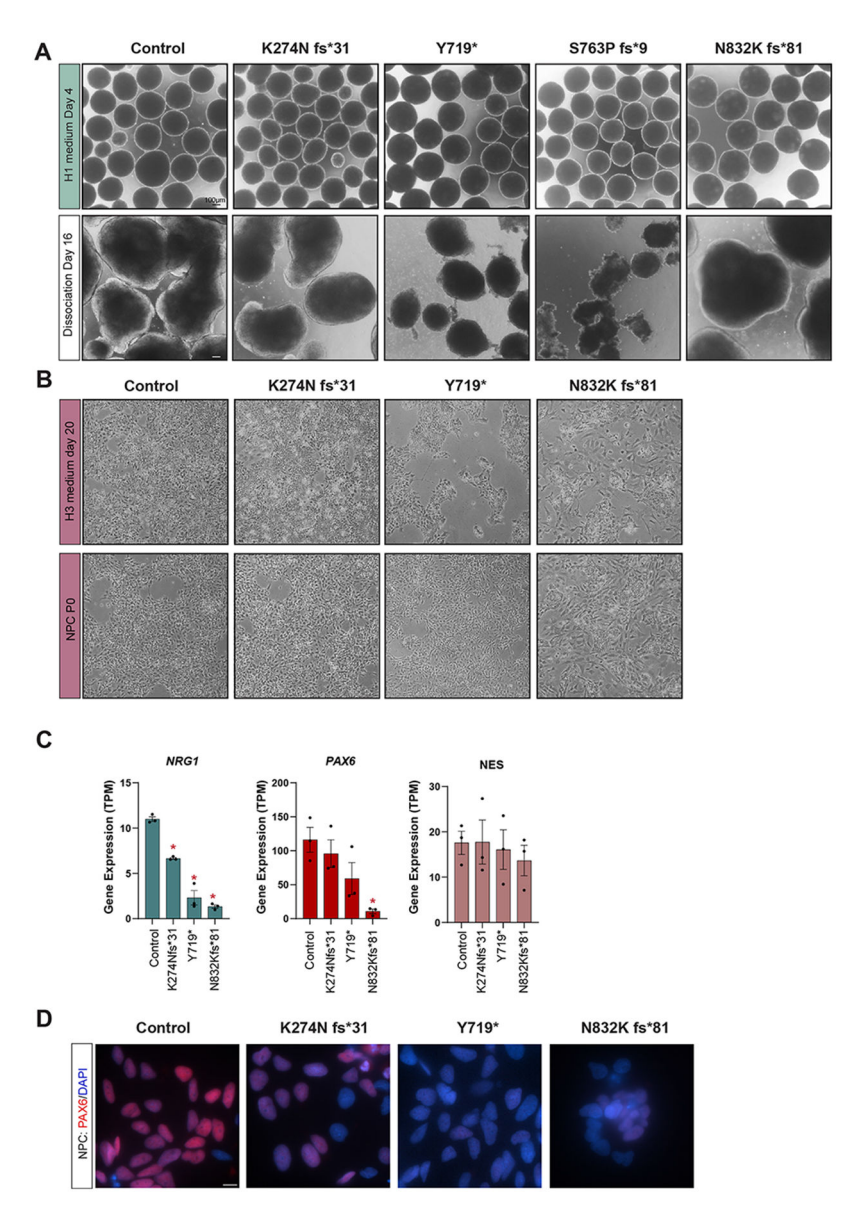


Figure 5. Effect of ADNP mutations on neurodifferentiation.

- A. Representative phase contrast images of Control, K274N fs*31, Y719*, S763P fs*9, and N832K fs*81 on day 4 (upper panel) and day 16 (lower panel) of 3D culture. Scale bar length is $100 \mu m$.
- B. Representative phase contrast images of Control, K274N fs*31, Y719*, S763P fs*9, and N832K fs*81 in the final stage of differentiation into NPCs.
- C. Bar plot showing expression of neural lineage markers *NRG1*, *PAX6*, and *NES* in transcripts per million (TPM) at the NPC stage in Control and mutants as indicated. Dots indicate 3 independent biological replicates. Data are presented as mean values +/– SEM. * p < 0.05, Welch's t-test.
- D. Immunostaining of Control, K274N fs*31, Y719*, and N832K fs*81 for PAX6 (red) and DAPI (blue) in NPC. Scale bar length is 10 μ m.

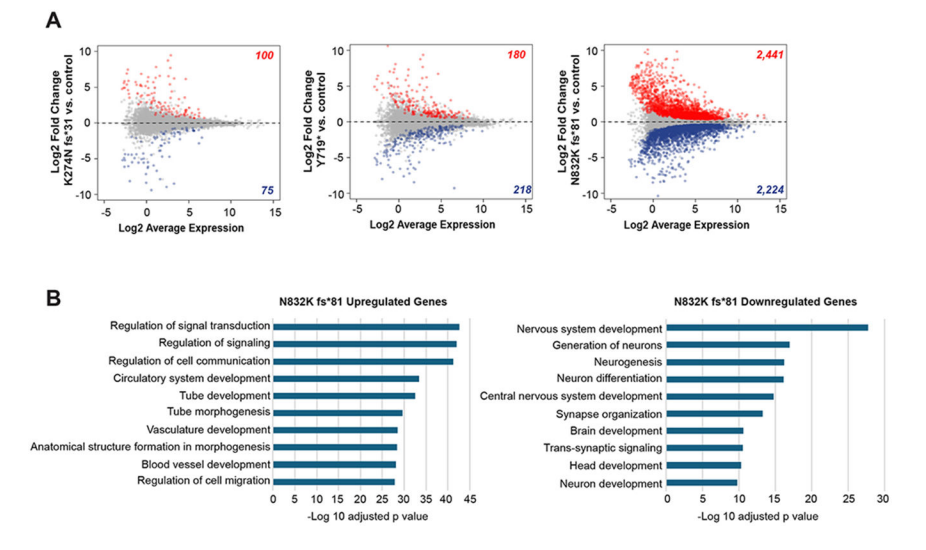


Figure 6. ADNP N832K fs*81 shows signatures of differentiation along the mesodermal lineage. A. MA plots of RNA-seq differential gene expression analyses between Control and ADNP mutants at the NPC stage, as indicated. Red dots and numbers indicate genes significantly upregulated in mutants (adjusted P-value $\,$ 0.05 and log2 fold change > 0). Blue dots and numbers indicate genes significantly downregulated in mutants (adjusted P-value $\,$ 0.05 and log2 fold change < 0).

B. Top 10 up- and down-regulated biological processes in N832K fs*81 at the NPC stage.

Table1.

ADNP mutant hiPSCs used in this study.

Mutant Name	Mutation in cDNA	Protein domain retained	Sex
K274N fs*31	c.819delC	4 ZnF	XY
Y719*	c.2156insA	9 ZnF	XY
S763P fs*9	c.2287delT	9 ZnF, NLS	XY
N832K fs*81	c.2496_2499 delTAAA	9 ZnF, NLS, HD	XY